Journal of Materials Chemistry A

ROYAL SOCIETY OF CHEMISTRY

PAPER

View Article Online
View Journal | View Issue

Check for updates

Cite this: J. Mater. Chem. A, 2025, 13, 5056

# Quick drying process: a promising strategy for preparing an egg-shell-type Cu/γ-$Al_2O_3$ catalyst for direct $N_2O$ decomposition†

Eun-Han Lee, [ab] In-Heon Kwak,[c] Hansung Kim *[b] and Shin-Kun Ryi *[a]

Received 31st October 2024
Accepted 30th December 2024

DOI: 10.1039/d4ta07764d

rsc.li/materials-a

The egg-shell-type γ-$Al_2O_3$ catalyst having a Cu shell was developed using the simple quick drying (QD) technique. The fabricated catalyst is developed for use in a direct $N_2O$ decomposition ($deN_2O$) technology. To observe the effective manufacturability of egg-shell-type catalysts, we compared three different drying methods: oven drying (OD), vacuum oven drying (VOD), and quick drying (QD). The SEM/EDS analysis, $deN_2O$ test, and kinetic properties (activation energy, reaction rate and turnover frequency) confirmed that the QD method is suitable for the effective manufacturability of the egg-shell-type catalyst. The simple QD method induces the formation of a thin and uniform Cu shell on the surface of the pellet support, which promotes $N_2O$ decomposition. A series of QD-Cu($x$)/γ-$Al_2O_3$ ($x$ = 5, 10, and 15 wt%) catalysts were prepared by the QD method. The QD-Cu(10)/γ-$Al_2O_3$ catalyst with an appropriate amount of Cu exhibited an outstanding $N_2O$ decomposition conversion rate and abundant $Cu^{1+}$ active sites with high reducibility. A long-term stability test with 1% and 20% $N_2O$ was carried out for 360 h and 500 h, respectively. During the long-term stability tests under changing feed conditions, such as temperature, air, and steam, the catalytic activity and copper distribution remained very stable, indicating that the QD-Cu(10)/γ-$Al_2O_3$ catalyst has high durability and reliability.

Open Access Article. Published on 08 January 2025. Downloaded on 9/16/2025 8:46:19 PM.
This article is licensed under a Creative Commons Attribution 3.0 Unported Licence.

## 1. Introduction

Nitrous oxide ($N_2O$) is a greenhouse gas with a global warming potential (GWP) of ~300 and a lifetime of 121 years.[1] Recent studies have shown that $N_2O$ has become the third most important greenhouse gas, followed by $CO_2$ and $CH_4$, due to its gradual increase in emissions yearly.[2] Even worse, the atmospheric concentration of $N_2O$ is gradually increasing and is expected to reach two times the current emissions by 2050 due to human activities.[3] Human activities that contribute to $N_2O$ emissions include biomass burning, fossil fuel combustion, industrial activities, *etc.*[4] $N_2O$ is usually emitted from adipic acid production tail gas, nitric acid production tail gas, three-way catalyst exhaust gas, and the direct use of ammonia as a fuel.[5] $N_2O$ emissions can be decreased in two ways: limiting the formation of $N_2O$ or after-treatment technologies.[6] Several after-treatment technologies have been developed and applied to control $N_2O$ emissions. These can be categorized into thermal decomposition,[7] non-selective catalytic reduction (NSCR),[8] selective catalytic reduction (SCR),[9,10] and direct decomposition ($deN_2O$).[4] Among them, $deN_2O$ (eqn (1)) has attracted great attention from due to its high decomposition efficiency, low energy consumption, economy, simplicity, and sustainability.[11,12]

$$2N_2O(g) \xrightarrow{\text{Catalyst}} 2N_2(g) + O_2(g) \quad \Delta H = -81.5\ \text{kJ mol}^{-1} \quad (1)$$

Various catalytic materials have been tested for $deN_2O$, including supported noble metals,[13,14] ion-exchanged zeolites,[15,16] and metal oxides.[17,18] Noble metal (such as Rh, Ir, Sm, *etc.*) doping in catalysts can improve $deN_2O$ activity while reducing the use of precious metals, and widespread industrial applications of noble metals are limited by their high cost and insufficient poisoning resistance. The ultimate goal in catalyst industries is to identify optimal earth-abundant materials.[13,14] Lucentini *et al.*[19] reported that there is a linear relationship between the price and GWP of a catalyst because it is related to the abundance of the element in the earth. For this reason, noble metals, such as Au, Pd, Pt, and Ru, have a high price and environmental impact. They also reported that using elements in the lower range, such as Al, Zn, Cu, Co, and Cr should be preferred. Therefore, there is a need to develop non-noble metal catalysts with improved catalytic activity and durability for practical applications.

[a]Korea Institute of Energy Research (KIER), 152 Gajeong-ro, Yuseong-gu, Daejeon 34129, Republic of Korea. E-mail: h2membrane@kier.re.kr
[b]Department of Chemical and Biological Engineering, Yonsei University, 50 Yonsei-ro, Seodaemun-gu, Seoul 03722, Republic of Korea. E-mail: elchem@yonsei.ac.kr
[c]Department of Chemical and Biological Engineering, Korea University, 145 Anam-ro, Seongbuk-gu, Seoul, Republic of Korea

† Electronic supplementary information (ESI) available. See DOI: https://doi.org/10.1039/d4ta07764d


This journal is © The Royal Society of Chemistry 2025

Open Access Article. Published on 08 January 2025. Downloaded on 9/16/2025 8:46:19 PM. This article is licensed under a Creative Commons Attribution 3.0 Unported Licence.

Numerous papers have reported that CuO has excellent performance and can achieve high redox, which is a prominent property for $N_2O$ decomposition.[20–22] Tanaka *et al.*[23] reported that the high activity of copper catalysts is quite interesting from a practical point of view, as copper catalysts have approximately the same activity as noble metals. Pekridis *et al.*[24] evaluated the performance of several metals, *i.e.*, Pd, Rh, Ru, Cu, Fe, In, and Ni supported on $\gamma$-$Al_2O_3$ catalysts, and it was concluded that noble metals (Pd, Ru, and Rh) followed by Cu exhibited the best catalytic performance.

According to the literature, various researchers have prepared catalysts in a uniform manner, *i.e.*, the active phase is homogeneously distributed in the support. If the active metals were selectively located on the outer part of the support, we could have reduced the characteristic diffusion distance by the classical 7 steps for heterogeneous catalysts and reduced the use of active metals.[25–27] From this perspective, egg-shell-type catalysts have been proposed for rapid reactions such as methane stream reforming,[28–30] Fischer–Tropsch synthesis,[31] purification of automobile exhaust gases,[32] and selective hydrogenation of pyrolysis gasoline.[33,34] Cho *et al.*[30] prepared an egg-shell-type Ni/Ru bimetallic alumina pellet catalyst by using the repulsion between hydrophobic 1-octanol and a hydrophilic ruthenium nitrosyl nitrate solution to selectively locate Ru in the outer region inside the alumina pellet. Similarly, Zhuang *et al.*[35] synthesized egg-shell catalysts using *n*-undecane as an organic solvent to prevent the distribution of the aqueous impregnation solution to the core of the pellet. Kim *et al.*[36] prepared a Ni-based egg-shell-type catalyst on cylindrical alumina pellets. To minimize the penetration of the hydrophilic solution containing Ni nitrate, they used a blocking solvent such as 1-octanol or ethylene glycol in the cylindrical pellet. The Ni precursors were then selectively loaded onto the pellet, and the hydrophobic and hydrophilic solvents were removed by drying. Xu *et al.*[37] used hydrophobic solvents to suppress the penetration of aqueous silver precursor solution into the pores of $SiO_2$ pellets.

So far, researchers have focused on blocking surface pores to prevent active metal solutions from settling into the pore. The application of these methods on a commercial scale is impeded by their additional process costs and non-scalable synthesis. In particular, the development of egg-shell-type catalysts without the use of chemical agents is challenging due to the rapid diffusion of the metal solution into the pores of the support. In the absence of a chemical agent to block the pores of the support, the thickness of the shell depends on the transport of the metal solution through a pore. In general, the drying rate can be affected by temperature and operating pressure.[38] Therefore, controlling the factors that determine the drying rate is a key point in designing egg-shell-type catalysts without chemical agents.

This study aims to improve the drying rate to prepare a thin egg-shell-type Cu/$\gamma$-$Al_2O_3$ catalyst for de$N_2O$ with high surface exposure of active metal, and to optimise the amount of Cu loading. First, three types of drying methods were compared to investigate the feasibility of controlling the egg-shell structure by using pressure and temperature: (1) oven drying (OD), (2) vacuum oven drying (VOD), and (3) quick drying (QD). SEM/EDS characterisation, the de$N_2O$ test, and kinetic properties (activation energy, reaction rate and turnover frequency (TOF)) showed that the QD process was the best method for preparing an egg-shell-type catalyst with fast solution evaporation rates. XPS, $H_2$-TPR analysis and the de$N_2O$ test indicated that the appropriate Cu content in the QD process was 10 wt%. The effects of oxygen, steam, and $N_2O$ concentration on the de$N_2O$ activity were verified. In addition, a long-term stability test for 360 and 500 h was performed to confirm the potential of the QD-Cu(10)/$\gamma$-$Al_2O_3$ catalyst to reduce $N_2O$ under various conditions, such as $N_2O$ concentration (1, 20%), steam (0–7.5%), oxygen, and temperature (500–650 °C). As a result, the QD-Cu(10)/$\gamma$-$Al_2O_3$ catalyst showed high durability without any degradation. Based on the results obtained in this study, it was suggested that the QD process has a high potential for fabricating effective egg-shell-type catalysts by a simple physical method and has a high potential for application as an industrial $N_2O$ decomposition catalyst.

## 2. Experimental section

### 2.1 Catalyst preparation

The $\gamma$-$Al_2O_3$ pellet (5 mm × 5 mm) supports were prepared by extrusion and heat treatment with boehmite (Sasol, high purity, 50 nm). The boehmite powder was mixed with deionized water in a plastic bag and extruded using a lab-scale table extruder as described in our previous study.[39] The extruded boehmite was dried at 80 °C for 12 h and calcined in a muffle furnace at 700 °C for 4 h. The Cu/$\gamma$-$Al_2O_3$ catalyst was prepared by spray coating followed by drying. The respective amounts of $Cu(NO_3)_2 \cdot 3H_2O$ (Sigma Aldrich) were dissolved in 20 mL of deionized water for the spray coating solution.

For the preparation of the egg-shell structured catalyst, three different methods were used to coat copper (Fig. 1). The OD method included spraying Cu solution and drying in an oven at 80 °C. The difference between the VOD method and OD was vacuum drying instead of oven drying. After spraying Cu solution on the surface of $\gamma$-$Al_2O_3$ pellets, the catalyst was dried in a vacuum drying oven at 80 °C at a gauge pressure of −100 kPa. The QD method involved spraying Cu solution and quick drying with a heat gun. The catalysts were then obtained by calcination at 500 °C for 4 h.

### 2.2 Catalytic performance tests

The schematic of the testing system is shown in Fig. S1,† which consisted of a vertical furnace, mass flow controllers (MFC, Alicat Co.), a water pump (NS, NP-KX-210) and a water trap. The $N_2O$ decomposition reaction was conducted in a 25.4 mm diameter Inconel 600 reactor packed with 20 mL of catalysts and placed in the center of a vertical furnace. $N_2O$ was supplied to be 1 or 20% by dry basis. In the case of steam effect testing, water was supplied by a water pump and vaporized in the preheating zone of the reactor. The conditions of the de$N_2O$ tests are shown in Table S1.† The concentration of $N_2O$ was analyzed by using

Open Access Article. Published on 08 January 2025. Downloaded on 9/16/2025 8:46:19 PM.
This article is licensed under a Creative Commons Attribution 3.0 Unported Licence.

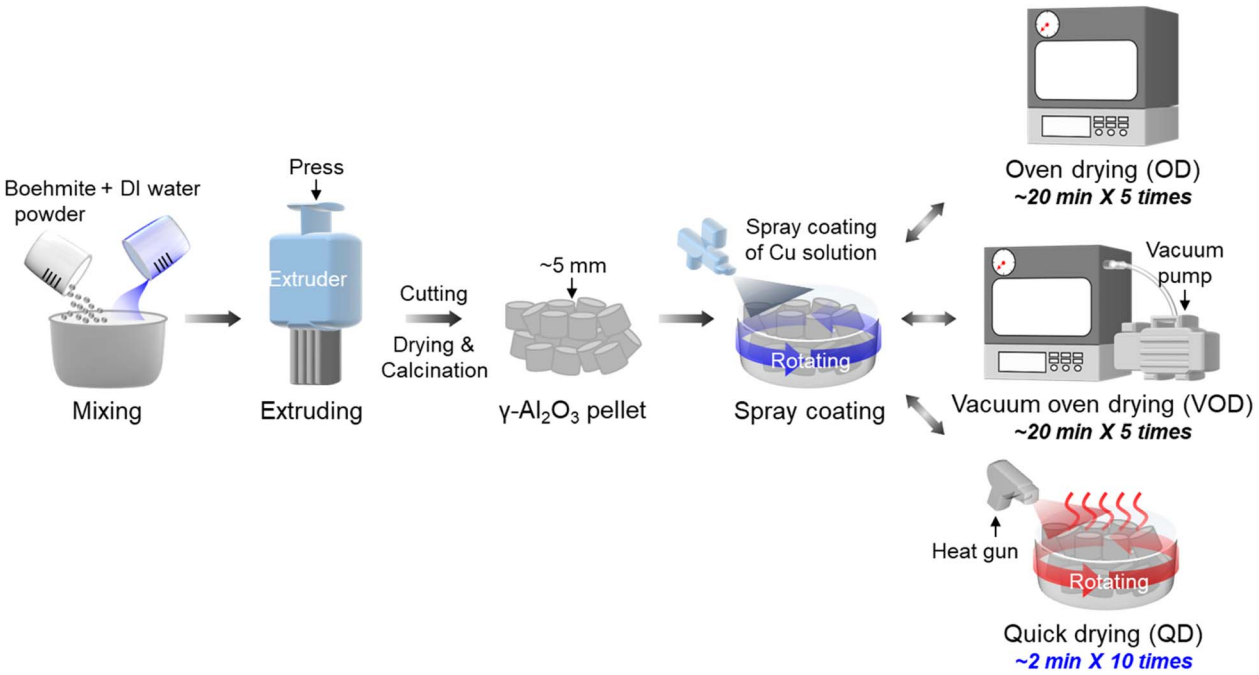


Fig. 1 Schematic illustration for the preparation process of γ-$Al_2O_3$, and three types of Cu/γ-$Al_2O_3$ catalysts.

a gas chromatograph equipped with an 80/100 Porapak Q column (6 ft, SS) and a thermal conductivity detector. The $NO_x$ (NO and $NO_2$) concentration at the outlet of the catalytic reactor was detected using NO and $NO_2$ detection tubes (Gastec Corporation). The $N_2O$ conversion rate was calculated by using the following equation:

$$N_2O\ \text{conversion rate} = \frac{(N_2O)_{in} - (N_2O)_{out}}{(N_2O)_{in}} \times 100 \quad (2)$$

where $(N_2O)_{in}$ and $(N_2O)_{out}$ represent the inlet and outlet $N_2O$ flow rates, respectively.

The activation energy ($E_a$) for the $N_2O$ decomposition was calculated by using the following equation:

$$k = -\frac{F_0 \ln(1-x)}{(N_2O) W_{cat}} \quad (2\text{-}1)$$

$$k = A \exp\left(-\frac{E_a}{RT}\right) \quad (2\text{-}2)$$

where $F_0$ (mol $s^{-1}$) is the total gas flow over the reaction reactor, $x$ is the $N_2O$ decomposition conversion, $(N_2O)$ (mol $cm^{-3}$) is the concentration of $N_2O$ at the inlet, $W_{cat}$ (g) is the amount of catalyst, $T$ (K) is the temperature, $A$ is the pre-exponential factor, and $R$ (8.314 J $mol^{-1}$ $K^{-1}$) is the gas constant.

Based on the specific surface area ($S_{BET}$), normalized reaction rates ($R_s$) were calculated by using the following equation:

$$R_s\left(\text{mol m}^{-2}\ \text{s}^{-1}\right) = -\frac{C_{inlet} F}{m_{cat.} S_{BET}} \ln(1 - X_{N_2O}) \quad (2\text{-}3)$$

where $C_{inlet}$ is $N_2O$ concentration in the inlet gas, $F$ (mol $s^{-1}$) is the flow rate, $m_{cat}$ (g) is the amount of catalyst, $S_{BET}$ ($m^2$ $g^{-1}$) is the specific surface area obtained by $N_2$ adsorption–desorption analysis, and $X_{N_2O}$ is the $N_2O$ decomposition efficiency.

The specific reaction rate ($r$) and turnover frequency (TOF) for $N_2O$ decomposition was calculated by using the following equation:

$$r\left(\mu\text{mol s}^{-1}\ g_{cat}^{-1}\right) = \frac{p_0 F 2000 \times 10^{-6}}{R T_0 m_{cat}} \times \text{Conv.}\% \quad (2\text{-}4)$$

$$\text{TOF}\left(s^{-1}\right) = \frac{r}{n} \quad (2\text{-}5)$$

where $p_0$ (101 325 Pa) is the atmospheric pressure, $F$ (ml $s^{-1}$) is the total flow rate of the feed gas mixture, $R$ (8.314 J $mol^{-1}$ $K^{-1}$) is the gas constant, $T_0$ (298 K) is room temperature, and $m_{cat}$ (g) is the amount of the catalyst. In eqn (2-5), $n$ (μmol $g_{cat}^{-1}$) is the amount of active sites detected by $O_2$-TPD.[2]

### 2.3 Catalyst characterization

A digital vernier caliper was used to measure the Cu shell thickness. Field emission scanning electron microscopy (FE-SEM, HITACHI S-4800) and energy dispersive X-ray spectroscopy (EDS, HORIVA XMAX 50) were used to determine the morphology images and Cu distribution. Surface areas and pore volumes were measured by the Brunauer–Emmett–Teller (BET, Micromeritics 3Flex 3500) method with $N_2$ adsorption–desorption at −196 °C. X-ray diffraction (XRD, Rigaku smartLab) patterns were obtained to identify the crystalline structures of the catalysts and the average particle size. The surface oxidation states of the Cu species were measured by the X-ray photoelectron spectroscopy (XPS, Thermo Fisher Scientific) method using Al Kα as the radiation source. The temperature programmed reduction of $H_2$ ($H_2$-TPR, MicrotracBEL Belcat 2)

 This journal is © The Royal Society of Chemistry 2025

Open Access Article. Published on 08 January 2025. Downloaded on 9/16/2025 8:46:19 PM. This article is licensed under a Creative Commons Attribution 3.0 Unported Licence.

analysis was performed to investigate the reducibility of the catalysts. Prior to the analysis, the catalysts were pretreated at 500 °C for 1 h in an atmosphere of helium to remove impurities. Then, the temperature was decreased to 50 °C, and 5 vol% $H_2$ + 95 vol% Ar mixture gas was supplied with 50 mL $min^{-1}$ instead of He. The temperature was increased to 1000 °C with a heating rate of 10 °C $min^{-1}$.

# 3. Results and discussion

## 3.1 Effect of the quick drying (QD) method on the preparation of egg-shell-type catalysts

In egg-shell-type catalysts, the active phase is located on the outer surface of the support. When an egg-shell-type catalyst is prepared using a porous catalyst, the metal solution can easily penetrate into the inner pores of the support. Therefore, to form the egg-shell structure, some researchers have tried to block the surface pores with chemical oils to prevent the metal solution from entering the inner pores of the support.[30,35–37] From the point of view of productivity, a very simple physical method should be considered. In this study, we prepared an egg-shell-type catalyst by spraying Cu solution on the γ-$Al_2O_3$ support to prevent the penetration of Cu solution into the inner pores of the γ-$Al_2O_3$ support. Then, we focused on the drying step to form the thin Cu shell structure, and three different drying methods were compared. Fig. 1 shows a schematic of three different drying methods. Oven drying (OD) is oven drying at 80 °C after spray coating with Cu solution. Vacuum oven drying (VOD) is a method of extracting the Cu solution that enters the internal pores after spraying in a vacuum environment, and the quick drying (QD) method is an attempt to rapidly dry the Cu solution before it enters the internal pores of the supports using a heat gun.

In the case of OD and VOD, we repeated the spraying and drying steps 5 times to complete the Cu coating. It took ~20 min to finish drying for each step, which means it took >100 min to complete the Cu coating. Using the QD method, the Cu coating was completed in 20 minutes with 10 repetitions of spraying and drying, which is an 80% reduction in manufacturing time compared to OD and VOD. Thus, when comparing catalyst productivity, it can be concluded that the QD method is the most efficient.

The uptake of the liquid into the pores of the support is due to the capillary pressure difference.[40] The Young–Laplace (Y–L) equation is widely used to describe the capillary pressure: $\Delta P = \gamma\left(\frac{1}{R_1}+\frac{1}{R_2}\right)$, where $\Delta P$ is the pressure difference across the liquid surface (the external pressure minus the internal pressure), $\gamma$ is the surface tension of the liquid, and $R_1$ and $R_2$ are the principal radii of surface curvature.[41] In a vacuum environment, the significantly reduced external pressure weakens the capillary pressure ($\Delta P$), preventing the liquid from entering the pores of the catalyst. In addition, as the temperature increases, the surface tension ($\gamma$) of water decreases due to a decrease in molecular attraction.[42] Therefore, as the temperature increases, the value of $\Delta P$ decreases (due to an increase in the internal pressure), which increases the pressure required for the liquid to enter the pore. Li *et al.*[38] found that the increase in the liquid temperature in the neighboring nanopore can significantly increase the net evaporation rate from the observed nanopore. Moreover, the evaporation mass flux increases with decreasing vapour pressure, because the condensation flow is minimised at lower vapour pressure. Therefore, the vacuum environment and high temperature help to prevent excessive penetration of the solution, ensuring that large amounts of Cu are deposited on the surface of the support. To investigate the variation of the Cu content on the support surface with the drying rate, egg-shell-type catalysts were prepared using different drying methods.

The γ-$Al_2O_3$ catalysts with Cu loading (1 wt%), denoted as OD-Cu(1)/γ-$Al_2O_3$, VOD-Cu(1)/γ-$Al_2O_3$, and QD-Cu(1)/γ-$Al_2O_3$ are derived from the drying methods (OD, VOD, and QD, respectively). As presented in the SEM images of OD-, VOD-, and QD-Cu(1)/γ-$Al_2O_3$ (Fig. 2a–c), although the same amount of 1 wt% Cu was supported on the γ-$Al_2O_3$ pellets, the Cu distribution on the surface varied depending on the drying method. Notably, QD-Cu(1)/γ-$Al_2O_3$ shows remarkably uniform and finely dispersed Cu particles. However, relatively few Cu particles were observed on the surface of oven and vacuum oven dried catalysts (OD-, VOD-Cu(1)/γ-$Al_2O_3$). The amount of Cu coating on the support surfaces was confirmed by using the Cu elemental mapping images using EDS (Fig. 2d). In the order of OD, VOD, and QD, more Cu particles appeared on the surface of γ-$Al_2O_3$. In particular, the Cu concentration on the surface was 10.47 wt% on the QD-Cu(1)/γ-$Al_2O_3$ catalyst, which was 31.7 and 3.8 times higher than that of OD- and VOD-Cu(1)/γ-$Al_2O_3$ catalysts, respectively. These results indicate that the use of vacuum drying or increasing the drying temperature can alleviate the penetration of the solution into the pore. In particular, the quick drying method can effectively prevent the Cu particles from penetrating into the support pores, while large amounts of active metal are deposited on the surface by increasing the evaporation rate of the metal solution.

BET analysis was carried out to examine whether the surface Cu coating obstructs the pores of the γ-$Al_2O_3$ support (Fig. 2e and S2†). OD-, VOD-, and QD-Cu(1)/γ-$Al_2O_3$ catalysts exhibited similar specific surface areas and pore volumes. As shown in Fig. S2a,† typical type IV curves with steep hysteresis loops were observed for the mesoporous structure. And the corresponding pore size distribution in Fig. S2b† shows that the pore size of γ-$Al_2O_3$ (13.4 nm) was similar to that of the OD-, VOD-, and QD-Cu(1)/γ-$Al_2O_3$ catalysts (11.6, 11.3, and 13.3 nm, respectively). This also suggests that the QD method can uniformly coat the active metal without affecting the pores and specific surface area of the support surface. As shown in Fig. 2f, the XRD patterns of the OD-, VOD-, and QD-Cu(1)/γ-$Al_2O_3$ catalysts indicated that all samples were assigned to γ-$Al_2O_3$ (JCPDS No. 29-0063). The absence of peaks belonging to the copper oxide phase can be explained by considering the fact that Cu particles are extremely small and well dispersed on the γ-$Al_2O_3$ surface.[43]

Fig. 3a shows a schematic diagram of the thick and thin egg-shell-type catalytic reaction mechanism. In a typical heterogeneous catalyst, the catalytic reaction occurs in seven classical steps (marked as reaction A):[26] (1) mass transfer of reactants to

Open Access Article. Published on 08 January 2025. Downloaded on 9/16/2025 8:46:19 PM.
This article is licensed under a Creative Commons Attribution 3.0 Unported Licence.

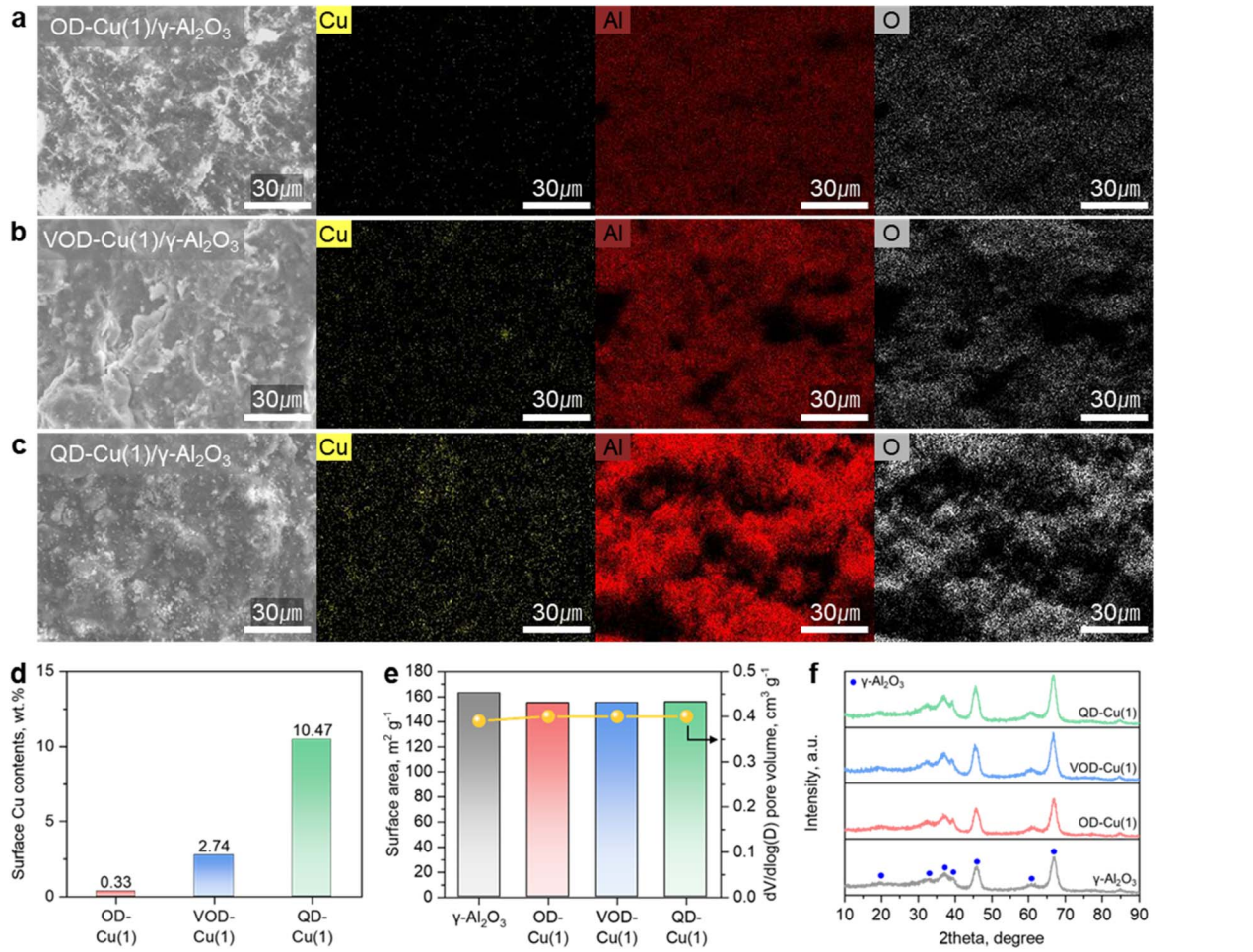


Fig. 2 Comparison of the physical properties of egg-shell-type catalysts. (a–c) FE-SEM/EDS mapping analysis and (d) surface Cu contents of the three types of catalysts. (e) $N_2$ adsorption–desorption results and (f) XRD patterns over γ-$Al_2O_3$ and OD-, VOD-, and QD-Cu(1)/γ-$Al_2O_3$ catalysts.

the catalyst surface, (2) diffusion of reactants from the pore entrance to the inner catalytic surface, (3) adsorption of reactants on the inner catalytic surface, (4) reaction at specific active sites on the catalyst surface, (5) desorption of the products from the inner surface, (6) diffusion of the products from the interior of the pellet to the pore entrance on the outer surface, and (7) diffusion of the products from the outer pellet surface to the bulk fluid. In reaction A, reducing the characteristic diffusion distance of the reactants can reduce the mass transfer resistance of the catalyst. The egg-shell structure is an attractive solution to independently shorten the diffusion length and maximize the reaction because the active metal is on the catalyst surface.[27] For this reason, egg-shell-type catalysts are dominated by the surface reaction that takes place on the loaded active metal (marked as reaction B). However, the shell thickness of egg-shell-type catalysts varies depending on the preparation method. When a thick egg-shell-type catalyst is prepared, it can be predicted that reactions A and B may occur similarly because the active metal is placed not only on the surface but also on the inside. In contrast, thin egg-shell-type catalysts are dominated by the surface reaction that takes place on the loaded active metal (reaction B).

To investigate the shell thickness according to the three different drying methods, the cross-sectional schematic and optical images of the OD-, VOD-, and QD-Cu(1)/γ-$Al_2O_3$ catalysts are shown in Fig. 3b. The Cu shell and support are well separated on the three different types of catalysts, indicating that the spray coating method is effective for preparing an egg-shell-type catalyst. The Cu shell thickness was varied with the different drying methods, and the average Cu shell thickness is ordered as follows: OD- (~1.00 mm) > VOD- (~0.66 mm) > QD- (~0.32 mm)Cu(1)/γ-$Al_2O_3$ catalysts (Fig. S3 and Table S2†). The thin Cu shell on the QD-Cu(1)/γ-$Al_2O_3$ catalyst reveals that a large amount of Cu particles are selectively located on the surface of the γ-$Al_2O_3$ support, combined with the SEM/EDS analysis (Fig. 2c and d).

To confirm the egg-shell structure, a cross-sectional SEM/EDS analysis of the QD-Cu(10)/γ-$Al_2O_3$ catalyst was carried out (Fig. S4†). The EDS line scan was performed at the boundary of the shell and support layer to verify the well formation of the Cu shell in detail, and the actual Cu shell thickness was investigated as shown in Fig. S3 and Table S2.† As shown in Fig. S4,† the Cu shell was well formed on the surface of the γ-$Al_2O_3$ support.

 This journal is © The Royal Society of Chemistry 2025

Open Access Article. Published on 08 January 2025. Downloaded on 9/16/2025 8:46:19 PM.
This article is licensed under a Creative Commons Attribution 3.0 Unported Licence.

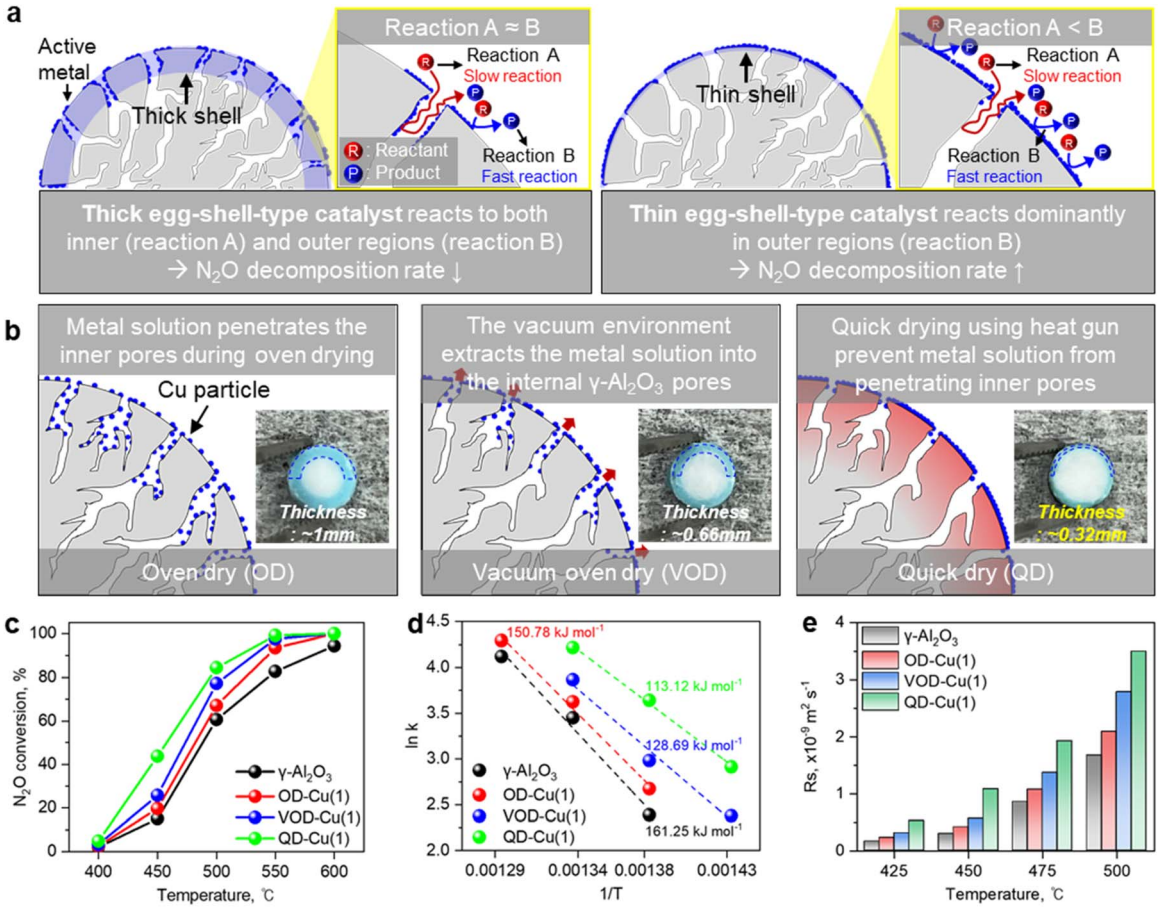


Fig. 3 Effect of the quick drying method on the preparation of egg-shell-type catalysts. (a) Schematic image of the catalytic reaction on the thick and thin egg-shell-type catalysts. (b) Cross-sectional schematic and optical images of the Cu particle distribution of the OD-, VOD-, and QD-catalysts. (c) $N_2O$ decomposition performance, (d) Arrhenius fitting curves, and (e) $S_{BET}$ normalised reaction rates over γ-$Al_2O_3$ and OD-, VOD-, and QD-Cu(1)/γ-$Al_2O_3$ catalysts. Reaction conditions: 20 mL catalyst, 1% $N_2O$, balance $N_2$, GHSV = 1800 $h^{-1}$.

To confirm the $N_2O$ decomposition activity as a function of shell thickness in the egg-shell-type catalyst, the de$N_2O$ activity was conducted under the case 1 condition in Table S1† (Fig. 3c). As shown in Fig. 3c, the de$N_2O$ activity was the highest in the order of QD-, VOD-, and OD-Cu(1)/γ-$Al_2O_3$ catalysts, supporting that the thinner egg-shell-type catalyst has higher de$N_2O$ activity. The activation energies ($E_a$) of the γ-$Al_2O_3$, OD-, VOD-, and QD-Cu(1)/γ-$Al_2O_3$ catalysts were calculated using the Arrhenius equation and are shown in Fig. 3d. The lower activation energy of the QD-Cu(1)/γ-$Al_2O_3$ catalyst than that of the γ-$Al_2O_3$, OD-, and VOD-Cu(1)/γ-$Al_2O_3$ catalysts proved that it is more favorable for the decomposition of $N_2O$ is to occur on the QD-Cu(1)/γ-$Al_2O_3$ catalyst. Furthermore, the reaction rate, normalised to the specific surface area, of $N_2O$ decomposition at different temperatures was calculated and is shown in Fig. 3e, and was consistent with the result that the QD-Cu(1)/γ-$Al_2O_3$ catalyst exhibited the highest catalytic activity. The TOF value of the OD-, VOD-, and QD-Cu(1)/γ-$Al_2O_3$ catalysts in the reaction process was calculated based on the integration area of $O_2$-TPD, which was $7.8 \times 10^{-5}$, $9.9 \times 10^{-5}$, and $1.6 \times 10^{-4}$, respectively (Table S3†).[2,44] The TOF values varied depending on the drying method, with the QD-Cu(1)/γ-$Al_2O_3$ catalyst exhibiting higher values than the OD- and VOD-Cu(1)/γ-$Al_2O_3$ catalysts, respectively. This means that the active metal located on the catalyst surface can react extremely to maximise the de$N_2O$ activity by uniformly forming a very thin Cu shell on the egg-shell-type catalyst. Therefore, although the same amount of Cu content was loaded on the γ-$Al_2O_3$ support, we could achieve high de$N_2O$ activity and effective kinetic properties on the QD-Cu(1)/γ-$Al_2O_3$ catalyst. Based on the results in Fig. 2 and 3, we can conclude that the spray coating method is a very simple and practical way to coat the active metal on the surface of the catalyst support, and the QD process is effective for de$N_2O$ activity by forming a thin and uniform shell in a short period of time.

### 3.2 Effect of Cu content on the γ-$Al_2O_3$ supports on $N_2O$ decomposition

The metal coated on the support surface significantly affects the physical properties of the catalyst and the gas decomposition rate, depending on the amount of coating. The Cu content was varied from 5, 10, and 15 wt% to investigate the effect of the metal content on the preparation of the QD-Cu($x$)/γ-$Al_2O_3$ catalysts. The dispersion and amount of Cu on the surface of the

Open Access Article. Published on 08 January 2025. Downloaded on 9/16/2025 8:46:19 PM.
This article is licensed under a Creative Commons Attribution 3.0 Unported Licence.

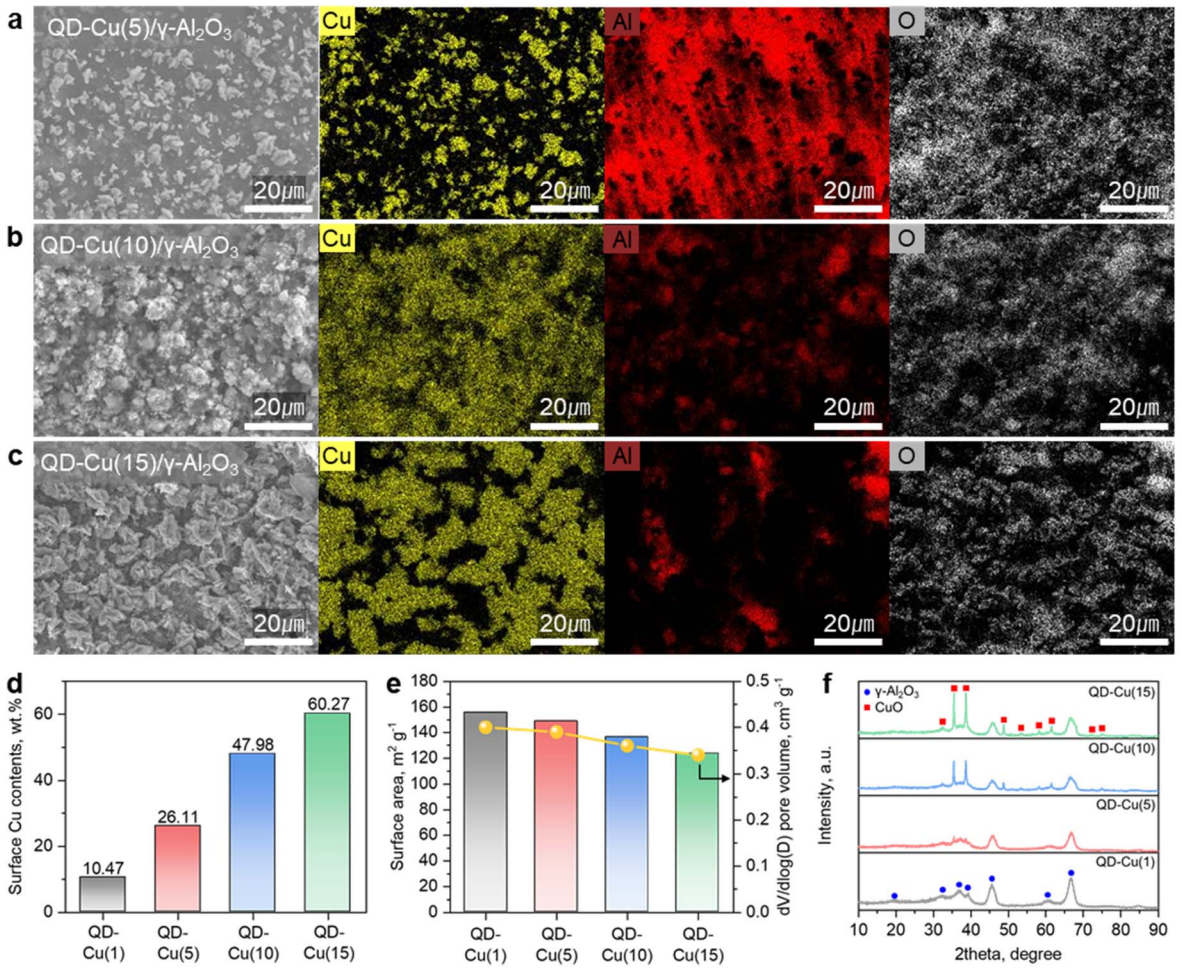


Fig. 4 Effect of Cu content on the γ-$Al_2O_3$ pellet on $N_2O$ decomposition. (a–c) FE-SEM/EDS mapping analysis of the 5, 10, and 15 wt% QD-Cu(*x*)/γ-$Al_2O_3$ catalyst surfaces. (d) Surface Cu contents, (e) $N_2$ adsorption–desorption results and (f) XRD patterns of the QD-Cu(*x*)/γ-$Al_2O_3$ catalysts (*x*: 1, 5, 10, 15 wt%).

γ-$Al_2O_3$ support were investigated by SEM (Fig. 4a–c). For QD-Cu(5)/γ-$Al_2O_3$ with 5 wt% Cu coating, Cu is unevenly coated on the support surface, whereas for QD-Cu(10)/γ-$Al_2O_3$ with 10 wt% Cu coating, dense Cu particles with uniform coating on the support surface can be seen. However, at a higher Cu coating of 15 wt% (QD-Cu(15)/γ-$Al_2O_3$), considerable Cu aggregation was observed (Fig. 4c). The amount of Cu coating on the γ-$Al_2O_3$ support surface was confirmed by EDS mapping analysis (Fig. 4d). The Cu content of QD-Cu(1)/γ-$Al_2O_3$ was only 10%, while for QD-Cu(15)/γ-$Al_2O_3$, 60% Cu was observed on the surface. It can also be seen that the Cu content on the surface increases proportionally with the amount of Cu coating. In addition, the Cu shell thickness was slightly changed with different Cu contents, and the average Cu shell thickness is ordered as follows: QD-Cu(15) (~0.40 mm) > QD-Cu(10) (~0.48 mm) > QD-Cu(5) (~0.54 mm) catalysts (Fig. S3 and Table S2†).

BET analysis was performed to investigate the effect of the Cu coating amount on the pores and surface area of the support (Fig. 4e). The surface area of QD-Cu(5)/γ-$Al_2O_3$ was 150 $m^2\ g^{-1}$, which was similar to that of QD-Cu(1)/γ-$Al_2O_3$ (155 $m^2\ g^{-1}$). However, at higher Cu coatings (10% and 15 wt%), the surface area was significantly lower than that of γ-$Al_2O_3$ (136 $m^2\ g^{-1}$ for QD-Cu(10)/γ-$Al_2O_3$, 123 $m^2\ g^{-1}$ for QD-Cu(15)/γ-$Al_2O_3$, and 163 $m^2\ g^{-1}$ for γ-$Al_2O_3$). The pore volume also tends to decrease with increasing Cu coating. This result suggests that excessive Cu coating blocks the pore volume of the support, thereby reducing the specific surface area.

The crystal structure of the QD-Cu(*x*)/γ-$Al_2O_3$ catalysts was determined by XRD analysis (Fig. 4f). In the case of the QD-Cu(1) and (5)/γ-$Al_2O_3$ catalysts, γ-$Al_2O_3$ formed the dominant peak due to the low Cu content on the surface, while a CuO peak (JCPDS No. 48-1548) was observed in QD-Cu(10) and (15)/γ-$Al_2O_3$ with a large amount of Cu coated on the surface. As the amount of Cu coating increased, the average particle size, calculated using the Scherrer's equation, increased from 17.2 nm (QD-Cu(10)/γ-$Al_2O_3$) to 22.2 nm (QD-Cu(15)/γ-$Al_2O_3$). Excessive Cu coating causes Cu particles to aggregate during high temperature heat treatment, resulting in an uneven surface distribution and a reduction in the active sites of the active metal. The average crystallite size of CuO for QD-Cu(1) and (5)/γ-$Al_2O_3$ is too small, so the size cannot be measured.

Correlations between the $N_2O$ decomposition activity and the relative abundance of $Cu^{1+}$ have been reported, as $Cu^{1+}$ can improve the catalytic activity.[43,45–47] As shown in eqn (3-1), the

 This journal is © The Royal Society of Chemistry 2025

Open Access Article. Published on 08 January 2025. Downloaded on 9/16/2025 8:46:19 PM. This article is licensed under a Creative Commons Attribution 3.0 Unported Licence.

$N_2O$ molecule interacts and adsorbs on the $Cu^{1+}$ site with the O atom. Such an interaction leads to weakening of the N–O bond, release of gas phase $N_2$ and oxidation of $Cu^{1+}$ to $Cu^{2+}$ (eqn (3-2)). Subsequently, a recombination step of two neighboring oxygen atoms is required to regenerate the initial $Cu^{1+}$ active site (eqn (3-3)).

$$Cu^{1+} + N_2O \rightarrow Cu^{1+} - ONN \quad (3\text{-}1)$$

$$Cu^{1+} - ONN \rightarrow Cu^{2+} - O^{-} + N_2 \quad (3\text{-}2)$$

$$Cu^{2+} - O^{-} \rightarrow 2Cu^{1+} + O_2 \quad (3\text{-}3)$$

The XPS analysis was carried out to investigate the oxidation states of the active Cu species on the surface of the catalysts. The XPS spectra of the Cu 2p core level at binding energies between 965 and 925 eV show the main and the satellite peaks of Cu $2p3_{/2}$ and Cu $2p_{1/2}$ over the QD-Cu($x$)/$\gamma$-$Al_2O_3$ catalysts (Fig. S5†). As shown in Fig. S5,† the spectra were fitted based on the intensity of the main peak of Cu $2p_{3/2}$. Copper oxide can exist in two semiconducting phases of $Cu_2O$ and CuO, *i.e.*, Cu in the +1 and +2 valence states, respectively. The peaks at 932.2–932.8 eV were assigned to the surface $Cu^{1+}$ species, while the peaks at 933.5–934.0 eV were assigned to the surface $Cu^{2+}$ species.[48–50] The relative abundances of $Cu^{1+}$ for QD-Cu($x$)/$\gamma$-$Al_2O_3$ ($x$: 5, 10, 15) were 32, 51, and 39%, respectively. These results indicated that $Cu^{1+}$ was the dominant species on the QD-Cu(10)/$\gamma$-$Al_2O_3$ catalyst surface.

The reducibility of the active site strongly influences the $N_2O$ decomposition activity.[51–53] $H_2$-TPR was performed to investigate the enhancement of the reducibility of the $\gamma$-$Al_2O_3$, QD-Cu(5), (10), and (15)/$\gamma$-$Al_2O_3$ catalysts (Fig. S6†). With the support of Cu species on the $\gamma$-$Al_2O_3$ catalyst, the reduction peak shifted to lower temperatures, which was attributed to the positive effects of the Cu support on the distribution over the surface of the $\gamma$-$Al_2O_3$ catalyst. These results indicate that the presence of Cu improves the reducibility of the $\gamma$-$Al_2O_3$ catalyst. In the $H_2$-TPR profile of the QD-Cu($x$)/$\gamma$-$Al_2O_3$ catalysts, there are two major reduction peaks at 150–300 °C, which correspond to the stepwise reduction of CuO to $Cu_2O$ and $Cu_2O$ to Cu.[54,55] The $H_2$-TPR profiles indicate that the QD-Cu(10)/$\gamma$-$Al_2O_3$ catalyst is easily reduced, followed by the Cu(15) and Cu(5)/$\gamma$-$Al_2O_3$ catalysts.

### 3.3 Catalytic activity test of the egg-shell-type QD-Cu(10)/$\gamma$-$Al_2O_3$ catalyst

The de$N_2O$ activity of as-prepared QD-Cu($x$)/$\gamma$-$Al_2O_3$ was evaluated at different reaction temperatures (Fig. 5a). At higher reaction temperatures, above 500 °C, the high activity of Cu resulted in 100% de$N_2O$ activation regardless of the Cu content, showing that the QD-Cu($x$)/$\gamma$-$Al_2O_3$ catalysts have remarkable activity. At the relatively low decomposition temperature of 400 and 450 °C, the de$N_2O$ activity was increased in the order QD-Cu(10) > (15) > (5)/$\gamma$-$Al_2O_3$. This observed trend is consistent with the Cu particle distribution results, indicating that the large amount of surface active metal induced by the uniform Cu coating has a positive effect on the de$N_2O$ activity, resulting in high efficiency even at low temperature (Fig. 4). Furthermore, the reducibility of the $H_2$-TPR results and abundance of $Cu^{1+}$ active site of XPS results are of the same order as the $N_2O$ decomposition activity. Based on the results of the de$N_2O$ activity test, we can conclude that 10 wt% Cu could be a reasonable amount when using the QD method to form an effective egg-shell-type catalyst.

The influence of varying gas mixtures and different concentrations of $N_2O$ on the catalytic activity of the QD-Cu(10)/$\gamma$-$Al_2O_3$ catalyst was also investigated (Fig. 5b and c). To determine the effect of oxygen and steam on the active site of the QD-Cu(10)/$\gamma$-$Al_2O_3$ catalyst, experiments were carried out under the conditions of case 2 and 3 in Table S1.† In general, the catalytic decomposition of $N_2O$ was highly dependent on the competitive adsorption between $O_2$ and $N_2O$ on the active sites of the catalysts.[14,17,20] Therefore, the presence of air strongly suppressed the active sites of the catalyst (Fig. 5b). For example, the $N_2O$ conversion curve was shifted to higher temperatures by about 70 °C due to the presence of $O_2$. However, as the temperature increased, the effect of $O_2$ decreased, and complete decomposition of $N_2O$ was achieved at 570 °C. The effect of $O_2$ and 7.5% $H_2O$ was investigated over the QD-Cu(10)/$\gamma$-$Al_2O_3$ catalyst (Fig. 5b). When $H_2O$ was further added to the feed side, the $N_2O$ conversion decreased drastically to 2.6% at 400 °C, and the complete conversion was achieved at 600 °C, which is 100 and 30 °C higher temperature than that in case 1 and 2, respectively. The presence of $H_2O$ in the de$N_2O$ reaction shows a more negative effect than $O_2$ due to competitive adsorption and poisoning of the catalyst active sites by $H_2O$.[56,57]

We have focused our research on $N_2O$ decomposition catalysts that can be used in the semiconductor and display manufacturing industries where sulphur oxides or nitrogen oxides are not emitted. Therefore, the influence of toxic substances such as $SO_x$ or $NO_x$ on the active sites of the QD-Cu(10)/$\gamma$-$Al_2O_3$ catalyst has not been determined. However, the influence of toxic substances could be expected. As reported in the literature, the addition of $SO_x$ to the feed stream results in severe irreversible deactivation.[58] Yu *et al.*[59] reported that the catalyst activity did not recover after the impurities (50 ppmv $SO_2$ + 5vol% $O_2$) were removed from the feed stream. In the case of $NO_x$, $NO_x$ strongly suppresses the active sites of the catalyst and has a severe inhibition effect compared to $O_2$ and $H_2O$.[2,57,59] Therefore, we believe that higher temperatures (above 650 °C) will be required for complete $N_2O$ decomposition in the presence of impurities such as $NO_x$ and $SO_x$. Currently, $NF_3$ and $SF_6$ are used as etching gases in semiconductors and display manufacturing processes, and we are researching catalysts for the simultaneous decomposition of $NF_3$, $SF_6$, and $N_2O$. Since $NF_3$ and $SF_6$ emit NO + $NO_2$ and $SO_x$ during hydrolysis, we will be able to determine the effects of $NO_x$ and $SO_x$ on $N_2O$ co-decomposition.[60,61] We plan to report on this study in detail in the future.

The use of greenhouse gases, such as fluorinated gases and $N_2O$ has increased with the growth of the electronics manufacturing industry.[62] $N_2O$ is used to remove organic contaminants from silicon wafer surfaces and for chamber-washing after chemical vapor deposition processes in

Open Access Article. Published on 08 January 2025. Downloaded on 9/16/2025 8:46:19 PM.
This article is licensed under a Creative Commons Attribution 3.0 Unported Licence.

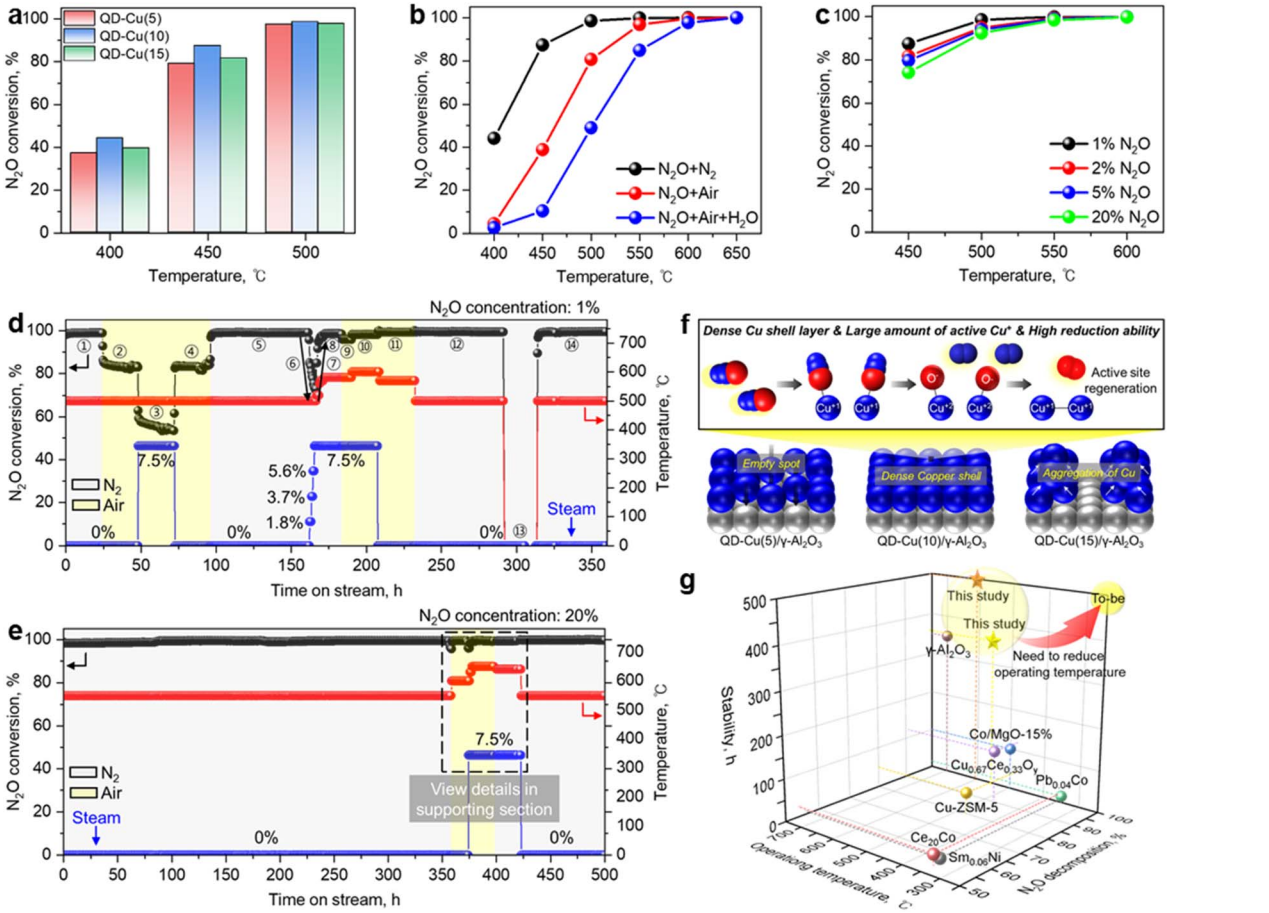


Fig. 5 Active test of the QD-Cu(10)/γ-$Al_2O_3$ catalyst. (a) $N_2O$ decomposition performance of the QD-Cu(*x*)/γ-$Al_2O_3$ catalysts (*x*: 5, 10, 15 wt%). (b) The effect of impurity gases and (c) different $N_2O$ contents as a function of the reaction temperature for the QD-Cu(10)/γ-$Al_2O_3$ catalyst. Reaction conditions: 20 mL catalyst, 1–20% $N_2O$, 5000 ppm $N_2O$, 0 or 7.5% $H_2O$, balance $N_2$ or air, GHSV = 1800 or 1960 $h^{-1}$. Long-term stability test over the QD-Cu(10)/γ-$Al_2O_3$ catalyst. (d) 1% and (e) 20% $N_2O$ concentration under different feed conditions with time on stream. (f) Schematic images of the $N_2O$ decomposition process on the QD-Cu(10)/γ-$Al_2O_3$ catalyst. (g) Comprehensive comparison with the reported catalytic performance for $N_2O$ decomposition.

semiconductor and liquid crystal display manufacturing.[62] In addition, $N_2O$ is also used in the chemical vapor deposition process to deposit an $SiO_2$ oxide film along with $SiH_4$.[63] In some cases, $N_2O$ emissions from semiconductors and display processes are as high as 15%. Therefore, the influence of different $N_2O$ concentrations (1–20%) over the QD-Cu(10)/γ-$Al_2O_3$ catalyst was also measured to verify the potential for reducing the high concentration of $N_2O$ emitted by the display industry using the conditions of case 4 in Table S1† (Fig. 5c). As shown in Fig. 5c, the catalytic efficiency tends to decrease under harsher feed gas conditions, but even under seriously harsh conditions using 20% $N_2O$, the QD-Cu(10)/γ-$Al_2O_3$ catalyst showed only a 14% performance decrease at 450 °C, still showing a high efficiency of 75%. However, at temperatures as high as 550 °C, the catalytic efficiency was over 99% even under 20% $N_2O$ supply, confirming that the prepared catalysts can exhibit high efficiencies even under harsh conditions.

Thus, the prepared QD-Cu(10)/γ-$Al_2O_3$ catalyst exhibited outstanding de$N_2O$ performance under various decomposition conditions. Long-term durability tests were also carried out to confirm the commercial suitability of the catalysts prepared by the QD method. In industry, $N_2O$ is emitted along with various impurities such as air and steam, and the $N_2O$ concentration is not constant. On this account, the de$N_2O$ reaction was carried out under different reaction conditions over ~360 h (Fig. 5d). Detailed information such as feed conditions, temperature, conversion rate, and the accumulation time with time on stream are also listed in Table S4.†

As shown in Fig. 5d, the $N_2O$ conversion remained stable at ~99% for ~24 h in the $N_2$ mixture (Section 1). When $N_2$ was changed to air and 7.5% $H_2O$ was injected into the inlet, the $N_2O$ conversion decreased to ~83% and ~54% (Sections 2 and 3), respectively, and the conversion value was maintained at ~54% (Section 3) for ~24 h. When the water injection was stopped, the catalytic activity recovered fully very quickly, indicating that the $H_2O$ inhibition is not permanent but reversible (Section 4). When $O_2$ was removed (Section 5), the catalytic activity recovered to the value in Section 1 and remained for 65 h. These results indicate that steam and oxygen do not induce drastic structural changes in our QD-Cu(10)/γ-$Al_2O_3$ catalyst.

 This journal is © The Royal Society of Chemistry 2025

Open Access Article. Published on 08 January 2025. Downloaded on 9/16/2025 8:46:19 PM. This article is licensed under a Creative Commons Attribution 3.0 Unported Licence.

The influence of $H_2O$ content is described in Section 6. The $N_2O$ conversion rate gradually decreased from ~99% to ~83%, ~78%, ~75%, and ~73% with increasing $H_2O$ contents of 1.8, 3.6, 5.4, and 7.5%, respectively. Surprisingly, when the $H_2O$ content exceeded 3.6%, the activity almost did not deteriorate with the $H_2O$ content. To verify the influence of temperature on the coexistence of steam, we increased the temperature from 500 °C to 580 °C, and the $N_2O$ conversion reached ~98%. Changing $N_2$ to air slightly decreased the conversion value due to $O_2$, but increasing the temperature to 600 °C increased the conversion rate to ~98%.

After turning off the water and replacing air with $N_2$, a similar $N_2O$ conversion rate of ~99% could be obtained at a lower temperature of ~70 °C, *i.e.*, 500 °C. The $N_2O$ conversion rate of ~99% was the same as that in Section 1. After ~60 h as in Section 12, the temperature was changed to room temperature with continuous feed gas to confirm the durability of the catalyst when the reactor is shut down due to electrical problems (Section 13). After remaining for ~22 h, when the temperature was then increased to 500 °C, the conversion value reached the same value of ~99% and was maintained for ~50 h (Section 14).

During the catalyst durability test, we checked the formation of $NO_x$ using NO and $NO_2$ detection tubes under different conditions, *i.e.*, $N_2$, $N_2$ + steam, and air + steam (Fig. S7†). No $NO_x$ was observed, indicating that the direct catalytic decomposition of $N_2O$ (eqn (1)) occurs completely on the QD-Cu(10)/γ-$Al_2O_3$ catalyst.

To confirm the applicability at high $N_2O$ concentration, the stability test was performed with 20% $N_2O$ for ~500 h. Detailed information such as supply conditions, temperature, conversion rate, and accumulation time with time on stream are given in Table S5.† The results in Fig. 5e indicate that the $N_2O$ conversion remained stable during the stability test. To verify the adaptability under different conditions, the gas compositions were changed after 355 h, and the temperatures were adjusted to achieve >99% conversion. The specific information from 350 to 430 h is provided in Fig. S8† As shown in Fig. S8,† when air was supplied instead of $N_2$, the $N_2O$ conversion dropped to ~95% due to the negative impact of $O_2$ (Section 2) and the conversion returned to ~99% at 600 °C (Sections 3 and 4). When 7.5% steam was injected into air, a complete decomposition can be obtained at 650 °C (Sections 5–7). After ~80 h of adaptability tests, the stability test under the $N_2$ + 20% $N_2O$ mixture was continued at 550 °C, and the catalytic activity remained stable for the last hours (Section 10). From the stability test with a high concentration of $N_2O$, it can be concluded that the QD-Cu(10)/γ-$Al_2O_3$ catalysts are very stable and applicable for high concentration of $N_2O$ and various feed conditions. After the stability test, SEM/EDS analysis was conducted for investigation of copper distribution on the surface of the support. The results in Fig. S9† indicate that the high copper dispersion still remained unchanged.

In summary, from the SEM surface analysis, XPS and $H_2$-TPR analysis, it can be concluded that the QD-Cu(10)/γ-$Al_2O_3$ catalyst exhibited excellent de$N_2O$ performance due to its highly dispersed Cu shell, abundant $Cu^{1+}$ active sites, and high reducibility (Fig. 5f). A comprehensive comparison with the reported catalytic performance for $N_2O$ decomposition is shown in Fig. 5g and Table S6.† The durability tests were carried out to demonstrate the commercial stability of the catalysts prepared by the QD method under 100% de$N_2O$ activity conditions. Although a 1 : 1 comparison with other reported literature is not possible due to different feed conditions, the durability tests indicated that the QD-Cu(10)/γ-$Al_2O_3$ catalyst exhibited excellent stability over long periods (~500 h) without degradation, even under very harsh conditions ($N_2O$ concentration: 20%). This result suggests that the catalyst prepared by the QD method is a promising candidate for commercial de$N_2O$ applications. In addition, through coating with synergistic metals (Ce, Co, *etc.*), surface functionalization, and heteroatom doping on the QD-manufactured egg-shell-type catalyst, we expect to develop catalysts with high decomposition efficiency at low temperatures and ensure commercial competitiveness.

## 4. Conclusions

In this work, egg-shell-type Cu/γ-$Al_2O_3$ catalysts were prepared by three different drying methods (oven drying (OD), vacuum oven drying (VOD), and quick drying (QD)), and their effects on the structure and performance of de$N_2O$ were investigated. SEM/EDS results clearly show that the QD method can significantly reduce the shell thickness by reducing the drying time of the metal solution penetrating into the pores of the γ-$Al_2O_3$ support. The highest de$N_2O$ performance, reaction rates ($1.08 \times 10^{-9}$ $m^2$ $s^{-1}$ at 450 °C) and TOF value ($1.6 \times 10^{-4}$ $s^{-1}$ at 450 °C) and lower activation energy (113.12 kJ $mol^{-1}$) were achieved when the QD method was adapted. The amount of Cu loading prepared by the QD method was optimised by comparing the surface active metal distribution, oxidation state of the active Cu species, reducibility, and the de$N_2O$ activity. SEM/EDS results reveal that the Cu in the QD-Cu(10)/γ-$Al_2O_3$ catalyst is highly dispersed and the Cu shell has high sintering resistance without agglomeration in long-term stability tests. Both XPS and $H_2$-TPR results illustrate that the QD-Cu(10)/γ-$Al_2O_3$ catalyst has abundant $Cu^{1+}$ (51%) active sites and high reducibility, thus facilitating the de$N_2O$ reaction. The QD-Cu(10)/γ-$Al_2O_3$ catalyst exhibited practical applicability in long-term stability tests (1% $N_2O$ for 360 h and 20% $N_2O$ for 500 h) without deactivation. The high stability and simple manufacturability of the QD-Cu(10)/γ-$Al_2O_3$ catalyst make the quick drying method an interesting candidate for industrial applications and the preparation of effective egg-shell-type catalysts.

## Data availability

The data supporting this article have been included as part of the ESI.†

## Author contributions

Eun-Han Lee: writing – original draft preparation, investigation. In-Heon Kwak: investigation. Hansung Kim: supervision, writing – review & editing. Shin-Kun Ryi: funding acquisition,

Open Access Article. Published on 08 January 2025. Downloaded on 9/16/2025 8:46:19 PM. This article is licensed under a Creative Commons Attribution 3.0 Unported Licence.

supervision, conceptualization, writing – review & editing, project administration.

## Conflicts of interest

There are no conflicts to declare.

## Acknowledgements

This work was conducted under the framework of the Research and Development Program of the Korea Institute of Energy Research (KIER) (C4-2475). This study was supported by the Korea Institute for Advancement of Technology (KIAT) World Class Plus project and received financial support from the Ministry of Trade, Industry & Energy, Republic of Korea (No. P0017165).

## References

1 Y.-K. Park and B.-S. Kim, *Chem. Eng. J.*, 2023, 461.
2 J. Qi, X. Qi, Y. Pan, J. Cui, Y. Xiong, W. Shan and H. Yu, *Appl. Surf. Sci.*, 2023, **611**, 155657.
3 Y. You, H. Chang, L. Ma, L. Guo, X. Qin, J. Li and J. Li, *Chem. Eng. J.*, 2018, **347**, 184–192.
4 M. Konsolakis, *ACS Catal.*, 2015, **5**, 6397–6421.
5 H. Liu, J. Chen, Y. Wang, S. Xiong, Z. Su, Y. Wang, W. Yang, X. Chu, W. Yang, Y. Peng, W. Si and J. Li, *Chem. Eng. J.*, 2021, 414.
6 F. Kapteijn, J. Rodriguez-Mirasol and J. A. Moulijn, *Appl. Catal., B*, 1996, **9**, 25–64.
7 M. Röhrig, E. L. Petersen, D. F. Davidson and R. K. Hanson, *Int. J. Chem. Kinet.*, 1996, **28**, 599–608.
8 J. Pérez-Ramírez, F. Kapteijn, K. Schöffel and J. A. Moulijn, *Appl. Catal., B*, 2003, **44**, 117–151.
9 X. Zhang, Q. Shen, C. He, C. Ma, J. Cheng, L. Li and Z. Hao, *ACS Catal.*, 2012, **2**, 512–520.
10 Y. You, S. Chen, J. Li, J. Zeng, H. Chang, L. Ma and J. Li, *J. Hazard. Mater.*, 2020, **383**, 121117.
11 X. Hu, Y. Wang, R. Wu and Y. Zhao, *Appl. Surf. Sci.*, 2021, **538**, 148157.
12 S. Hinokuma, T. Iwasa, Y. Kon, T. Taketsugu and K. Sato, *Sci. Rep.*, 2020, **10**, 21605.
13 V. K. Tzitzios and V. Georgakilas, *Chemosphere*, 2005, **59**, 887–891.
14 S. Parres-Esclapez, M. J. Illán-Gómez, C. S.-M. de Lecea and A. Bueno-López, *Appl. Catal., B*, 2010, **96**, 370–378.
15 H. Xia, K. Sun, Z. Liu, Z. Feng, P. Ying and C. Li, *J. Catal.*, 2010, **270**, 103–109.
16 B. M. Abu-Zied, W. Schwieger and A. Unger, *Appl. Catal., B*, 2008, **84**, 277–288.
17 Z. Liu, F. He, L. Ma and S. Peng, *Catal. Surv. Asia*, 2016, **20**, 121–132.
18 A. Satsuma, H. Maeshima, K. Watanabe, K. Suzuki and T. Hattori, *Catal. Today*, 2000, **63**, 347–353.
19 I. Lucentini, X. Garcia, X. Vendrell and J. Llorca, *Ind. Eng. Chem. Res.*, 2021, **60**, 18560–18611.
20 S. Choi, K. Bok Nam, H. Phil Ha and D. Wook Kwon, *J. Ind. Eng. Chem.*, 2023, **121**, 462–471.
21 S. Kawi, S. Y. Liu and S. C. Shen, *Catal. Today*, 2001, **68**, 237–244.
22 C. Ohnishi, K. Asano, S. Iwamoto, K. Chikama and M. Inoue, *Catal. Today*, 2007, **120**, 145–150.
23 K. Tanaka, A. Shimizu, M. Fujimori, S. Kodama and S. Sawai, *Bull. Chem. Soc. Jpn.*, 2003, **76**, 651–657.
24 G. Pekridis, C. Athanasiou, M. Konsolakis, I. V. Yentekakis and G. E. Marnellos, *Top. Catal.*, 2009, **52**, 1880.
25 V. Russo, L. Mastroianni, R. Tesser, T. Salmi and M. Di Serio, *Chem. Eng.*, 2020, **4**, 24.
26 R. Klaewkla, M. Arend and W. F. Hoelderich, *A Review of Mass Transfer Controlling the Reaction Rate in Heterogeneous Catalytic Systems*, INTECH Open Access Publisher, Rijeka, 2011.
27 C. Niu, H. Li, M. Xia, J. Wang, C. Chen, Z. Ma, L. Jia, B. Hou and D. Li, *AIChE J.*, 2021, **67**, e17226.
28 E. Cho, Y. J. Yu, Y. Kim, T. N. Phan, D. Park and C. H. Ko, *Catal. Today*, 2020, **352**, 157–165.
29 K. Takehira, T. Shishido, D. Shoro, K. Murakami, M. Honda, T. Kawabata and K. Takaki, *Catal. Commun.*, 2004, **5**, 209–213.
30 E. H. Cho, K. Y. Koo, H. W. Lee, Y.-K. Park, W. L. Yoon and C. H. Ko, *Int. J. Hydrogen Energy*, 2017, **42**, 18350–18357.
31 S. A. Gardezi, J. T. Wolan and B. Joseph, *Appl. Catal., A*, 2012, **447–448**, 151–163.
32 B. Liu, Y. Chai, Y. Liu, Y. Wang, Y. Liu and C. Liu, *Fuel*, 2012, **95**, 457–463.
33 X. Wen, R. Li, Y. Yang, J. Chen and F. Zhang, *Appl. Catal., A*, 2013, **468**, 204–215.
34 Z. Zhou, T. Zeng, Z. Cheng and W. Yuan, *Chem. Eng. Sci.*, 2010, **65**, 1832–1839.
35 Y. Q. Zhuang, M. Claeys and E. van Steen, *Appl. Catal., A*, 2006, **301**, 138–142.
36 Y. Kim, E. Cho and C. H. Ko, *Int. J. Hydrogen Energy*, 2019, **44**, 5314–5323.
37 X. Xu, X. Hu, Z. Luo, Y. Cao, Y.-A. Zhu, W. Li, J. Zhou and X. Zhou, *New J. Chem.*, 2023, **47**, 6045–6049.
38 R. Li, Z. Yan and G. Xia, *Phys. Fluids*, 2023, **35**, 032015.
39 E.-H. Lee, T.-W. Kim, S. Byun, D.-W. Seo, H.-J. Hwang, J. Baek, E.-S. Jeong, H. Kim and S.-K. Ryi, *Clean Technol.*, 2023, **29**, 126–134.
40 P. Munnik, P. E. De Jongh and K. P. De Jong, *Chem. Rev.*, 2015, **115**, 6687–6718.
41 H. Liu and G. Cao, *Sci. Rep.*, 2016, **6**, 23936.
42 Y. Huang, X. Zhang, Z. Ma, Y. Zhou, W. Zheng, J. Zhou and C. Q. Sun, *Coord. Chem. Rev.*, 2015, **285**, 109–165.
43 M. Zabilskiy, P. Djinović, B. Erjavec, G. Dražić and A. Pintar, *Appl. Catal., B*, 2015, **163**, 113–122.
44 F. Zhang, X. Wang, X. Zhang, M. Tursun and H. Yu, *Chin. J. Catal.*, 2015, **36**, 344–347.
45 A. Dandekar and M. Vannice, *Appl. Catal., B*, 1999, **22**, 179–200.
46 M. Zabilskiy, P. Djinović, E. Tchernychova, O. P. Tkachenko, L. M. Kustov and A. Pintar, *ACS Catal.*, 2015, **5**, 5357–5365.

 This journal is © The Royal Society of Chemistry 2025

Open Access Article. Published on 08 January 2025. Downloaded on 9/16/2025 8:46:19 PM.
This article is licensed under a Creative Commons Attribution 3.0 Unported Licence.

47 P. Xie, Z. Ma, H. Zhou, C. Huang, Y. Yue, W. Shen, H. Xu, W. Hua and Z. Gao, *Microporous Mesoporous Mater.*, 2014, **191**, 112–117.
48 D. S. Kozak, R. A. Sergiienko, E. Shibata, A. Iizuka and T. Nakamura, *Sci. Rep.*, 2016, **6**, 21178.
49 D. Tahir and S. Tougaard, *J. Phys.: Condens. Matter*, 2012, **24**, 175002.
50 S. Poulston, P. Parlett, P. Stone and M. Bowker, *Surf. Interface Anal.*, 1996, **24**, 811–820.
51 L. Chen, H. Chen, J. Lin and K. Tan, *Surf. Interface Anal.*, 1999, **28**, 115–118.
52 S. Xiong, J. Chen, N. Huang, S. Yang, Y. Peng and J. Li, *Surf. Interface Anal.*, 2019, **53**, 10379–10386.
53 H. Zhou, Z. Huang, C. Sun, F. Qin, D. Xiong, W. Shen and H. Xu, *Appl. Catal., B*, 2012, **125**, 492–498.
54 Y. Li, X. Wang and C. Shi, *J. Environ. Chem. Eng.*, 2023, **11**, 109970.
55 M. Konsolakis, S. A. C. Carabineiro, E. Papista, G. E. Marnellos, P. B. Tavares, J. A. Moreira, Y. Romaguera-Barcelay and J. L. Figueiredo, *Catal. Sci. Technol.*, 2015, **5**, 3714–3727.
56 M. Tursun, X. Wang, F. Zhang and H. Yu, *Catal. Commun.*, 2015, **65**, 1–5.
57 S. Parres-Esclapez, M. Illán-Gómez, C. S.-M. de Lecea and A. Bueno-López, *Int. J. Greenhouse Gas Control*, 2012, **11**, 251–261.
58 M. Konsolakis, I. V. Yentekakis, G. Pekridis, N. Kaklidis, A. C. Psarras and G. E. Marnellos, *Appl. Catal., B*, 2013, **138–139**, 191–198.
59 H. Yu, M. Tursun, X. Wang and X. Wu, *Appl. Catal., B*, 2016, **185**, 110–118.
60 N.-K. Park, Y. H. Jeong, J. W. Lee and T. J. Lee, *Catal. Today*, 2018, **303**, 46–54.
61 D. Liu, Y. Gui, C. Ji, C. Tang, Q. Zhou, J. Li and X. Zhang, *Appl. Surf. Sci.*, 2019, **465**, 172–179.
62 S. J. Lee, I. S. Ryu and S. H. Moon, *Greenhouse Gases:Sci. Technol.*, 2012, **2**, 380–385.
63 D. K. Kim, Y. K. Park, S. Biswas and C. Lee, *Mater. Chem. Phys.*, 2005, **91**, 490–493.